Progress In Electromagnetics Research, Vol. 139, 577–597, 2013

IMPLEMENTATION AND APPLICATION OF THE SPHERICAL MRTD ALGORITHM

Yawen Liu*, Yiwang Chen, Pin Zhang, and Xin Xu

National Key Laboratory on Electromagnetic Environment and Electro-optical Engineering, PLA University of Science and Technology, Nanjing 210007, China

Abstract—This paper illustrates an explicit multiresolution time-domain (MRTD) scheme based on Daubechies' scaling functions with a spherical grid for time-domain Maxwell's equations. The stability and dispersion property of the scheme are investigated and it is shown that larger cells decrease the numerical phase error, which makes it significantly lower than FDTD for low and medium discretizations. Moreover, this technique is applied to the modeling of an air-filled spherical resonator and the propagation of a radiating electric dipole in spherical coordinates, numerical results demonstrate the effectiveness of the proposed algorithm.

1. INTRODUCTION

The Multi-Resolution Time-Domain (MRTD) technique was first published in 1996 by Krumpholz and Katehi [1], and has been developed rapidly as an efficient numerical algorithm in the time-domain like the long established Finite Difference Time-Domain (FDTD) technique [2–16] and other time-domain methods [17–19]. With highly-linear dispersion performance, the MRTD scheme implies that a low sampling rate in space can still provide for a relatively small phase error in the numerical simulation of a wave propagation problem, so it becomes possible that larger targets can be simulated without sacrificing accuracy. This paper extends the MRTD concept to spherical coordinates, and presents a MRTD algorithm for solving Maxwell equations in spherical grids, considering that some problems in antenna design and ultra-close-in coupling can be better solved in spherical coordinates with azimuthal dependence.

Received 1 April 2013, Accepted 29 April 2013, Scheduled 10 May 2013

* Corresponding author: Yawen Liu (liuyawen1111@163.com).

The initial works in [1] applied cubic spline Battle-Lemarie scaling and wavelet functions in the spatial domain, while keeping rectangular-pulse basis functions for the time domain. Then different wavelet bases such as Haar, Coifman, Daubechies, and Cohen-Daubechies-Feauveau (CDF) were introduced for the MRTD method. Since the cubic spline Battle-Lemarie wavelet function is not compactly supported in the spatial domain, it brings quantity of field coefficients and makes the calculation complex. In order to reduce the number of the considering items, a compactly supported wavelet can be used as an alternative basis. So in this work, the compact support wavelet-Daubechies with two vanishing moments (D_2) [20, 21] is employed to the spherical MRTD, the stability and dispersion characteristic of the scheme is also analyzed and compared with that of the FDTD scheme. Furthermore, the numerical simulations prove the applicability of the spherical MRTD method.

2. MRTD FOR SPHERICAL GRID

For simplicity and compactness, a homogeneous medium is considered. Faraday's and Ampere's laws in Maxwell's equations are stated by

$$\nabla \times \mathbf{E} = -\mu \frac{\partial \mathbf{H}}{\partial t}, \qquad \nabla \times \mathbf{H} = \varepsilon \frac{\partial \mathbf{E}}{\partial t} \tag{1}$$

The MRTD solution of Maxwell's equations requires the discretization of Eq. (1). In spherical coordinates, Eq. (1) can be rewritten as

$$\varepsilon \frac{\partial E_r}{\partial t} + \sigma E_r = \frac{1}{r \sin\theta} \left[\frac{\partial (\sin\theta H_\varphi)}{\partial \theta} - \frac{\partial H_\theta}{\partial \varphi} \right] \tag{2}$$

$$\varepsilon \frac{\partial E_\theta}{\partial t} + \sigma E_\theta = \frac{1}{r} \left[\frac{1}{\sin\theta} \frac{\partial H_r}{\partial \varphi} - \frac{\partial (r H_\varphi)}{\partial r} \right] \tag{3}$$

$$\varepsilon \frac{\partial E_\varphi}{\partial t} + \sigma E_\varphi = \frac{1}{r} \left[\frac{\partial (r H_\theta)}{\partial r} - \frac{\partial H_r}{\partial \theta} \right] \tag{4}$$

$$-\mu \frac{\partial H_r}{\partial t} - \sigma_m H_r = \frac{1}{r \sin\theta} \left[\frac{\partial (\sin\theta E_\varphi)}{\partial \theta} - \frac{\partial E_\theta}{\partial \varphi} \right] \tag{5}$$

$$-\mu \frac{\partial H_\theta}{\partial t} - \sigma_m H_\theta = \frac{1}{r} \left[\frac{1}{\sin\theta} \frac{\partial E_r}{\partial \varphi} - \frac{\partial (r E_\varphi)}{\partial r} \right] \tag{6}$$

$$-\mu \frac{\partial H_\varphi}{\partial t} - \sigma_m H_\varphi = \frac{1}{r} \left[\frac{\partial (r E_\theta)}{\partial r} - \frac{\partial E_r}{\partial \theta} \right] \tag{7}$$

Also for the sake of simplicity and without loss of generality, the electric and magnetic fields are expanded in terms of scaling functions

only in space domain and pulse functions in time domain.

$$E_r(\mathbf{v},t)=\sum_{i,j,k,n=-\infty}^{+\infty} E_{i+1/2,j,k}^{\phi r,\,n} h_n(t)\phi_{i+1/2}(r)\phi_j(\theta)\phi_k(\varphi) \tag{8}$$

$$E_\theta(\mathbf{v},t)=\sum_{i,j,k,n=-\infty}^{+\infty} E_{i,j,k+1/2}^{\phi\theta,\,n} h_n(t)\phi_i(r)\phi_{j+1/2}(\theta)\phi_k(\varphi) \tag{9}$$

$$E_\varphi(\mathbf{v},t)=\sum_{i,j,k,n=-\infty}^{+\infty} E_{i,j+1/2,k}^{\phi\varphi,\,n} h_n(t)\phi_i(r)\phi_j(\theta)\phi_{k+1/2}(\varphi) \tag{10}$$

$$H_r(\mathbf{v},t)=\sum_{i,j,k,n=-\infty}^{+\infty} H_{i,j+1/2,k+1/2}^{\phi r,n+1/2} h_{n+1/2}(t)\phi_i(r)\phi_{j+1/2}(\theta)\phi_{k+1/2}(\varphi) \tag{11}$$

$$H_\theta(\mathbf{v},t)=\sum_{i,j,k,n=-\infty}^{+\infty} H_{i+1/2,j,k+1/2}^{\phi z,n+1/2} h_{n+1/2}(t)\phi_{i+1/2}(r)\phi_j(\theta)\phi_{k+1/2}(\varphi) \tag{12}$$

$$H_\varphi(\mathbf{v},t)=\sum_{i,j,k,n=-\infty}^{+\infty} H_{i+1/2,j+1/2,k}^{\phi\varphi,n+1/2} h_{n+1/2}(t)\phi_{i+1/2}(r)\phi_{j+1/2}(\theta)\phi_k(\varphi) \tag{13}$$

where $E_{i,j,k}^{\phi\kappa,\,n}$ and $H_{i,j,k}^{\phi\kappa,\,n}$, with $\kappa = r,\theta,\varphi$, are the coefficients for the fields expansions in terms of scaling functions. The indexes i, j, k and n are the discrete space and time indices related to the space and time coordinates via $r = i\Delta r$, $\theta = j\Delta\theta$, $\varphi = k\Delta\varphi$ and $t = n\Delta t$, where Δr, $\Delta\theta$, $\Delta\varphi$ and Δt, represent the space and time discretization intervals in r-, θ-, φ- and t-direction. The function $h(t)$ is defined as Haar's scaling function, and $\phi(v)$ is Daubechies' scaling function. Moreover, the functions of $h_n(t)$ and $\phi_m(v)$ are defined by

$$h_n(t) = h\left(\frac{t}{\Delta t} - n\right) \tag{14}$$

$$\phi_m(x) = \phi\left(\frac{v}{\Delta v} - m\right), \qquad v = \rho,\varphi,z \tag{15}$$

The Daubechies scaling function with two vanishing wavelet moments (D_2) is shown in Fig. 1.

Substituting (8)–(13) to (2)–(7) and applying Galerkin scheme and wavelet function as following:

$$\left\langle h_m(x),\ \frac{\partial h_{m'+1/2}(x)}{\partial x}\right\rangle = \delta_{m,\,m'} - \delta_{m,\,m'+1} \tag{16}$$

$$\left\langle \varphi_m(x),\ \varphi'_m(x)\right\rangle = \delta_{m,\,m'}\Delta x \tag{17}$$

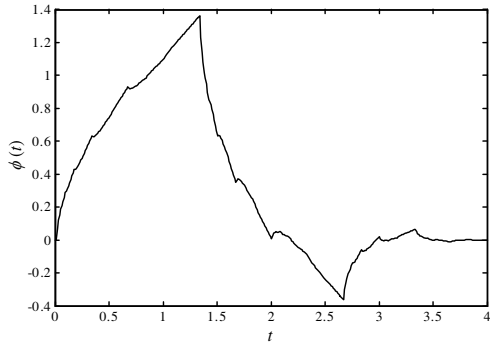

Figure 1. Daubechies scaling function with two vanishing moment.

$$\left\langle \varphi_m(x),\ \frac{\partial \varphi_{m'+1/2}(x)}{\partial x} \right\rangle = \sum_l a(l)\delta_{m+l,\,m'} \tag{18}$$

As remarked by mathematicians [22], the shifted Daubechies D_2 scaling functions has approximate sampling properties. Therefore (15) is modified to

$$\phi_i\left(\frac{x}{\Delta x} - i + M_1\right) = \delta_{k,0} \tag{19}$$

where $M_1 = \int_{-\infty}^{+\infty} x\phi(x)dx$ is the first-order moment of the scaling function and δ is the Kronecker delta function. This property yields a simple algorithm for inhomogeneous problems through the local sampling of the field values regardless of the complexity of the inhomogeneity [20]. The coefficients $a(l)$ for $0 \le l \le 2$ are shown in Table 1 together with the first-order moment M_1, and for $l > 2$, $a(l)$ are zeros due to the compact support of Daubechies' scaling function. The coefficients $a(l)$ for $l < 0$ are given by the symmetry relation $a(-1-l) = -a(l)$.

As shown in Fig. 2, the unit cell of the MRTD scheme is similar to the unit cell of the spherical Yee grid. However, due to the different

Table 1. The coefficients $a(l)$ and the first-order moments M_1.

l	$a(l)$
0	1.22916661202745
1	−0.09374997764746
2	0.01041666418309
M_1	0.6339743121

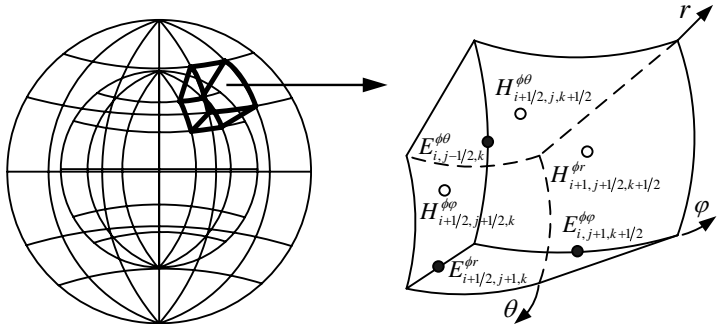

Figure 2. A nonuniform spherical unit cell for the MRTD scheme.

field expansions, the field components in the two schemes are not identical. Take E_r as example, the component of which at point $((i+1/2)\Delta\rho,\, j\Delta\theta,\, k\Delta\varphi,\, n\Delta t)$ is given by

$$\begin{aligned} & E_r\left((i+1/2)\,\Delta r, j\Delta\theta, k\Delta\varphi, n\Delta t\right) \\ = & \int_{-\infty}^{\infty}\int_{-\infty}^{\infty}\int_{-\infty}^{\infty}\int_{-\infty}^{\infty} E_\rho\left(\mathbf{r},t\right)\delta\left(\frac{r}{\Delta r}-i-\frac{1}{2}\right) \\ & \cdot\delta\left(\frac{\theta}{\Delta\theta}-j\right)\delta\left(\frac{\varphi}{\Delta\varphi}-k\right)\delta\left(\frac{t}{\Delta t}-n\right) r dr d\theta d\varphi dt = E^{\phi r,n}_{i+1/2,j,k} \end{aligned} \tag{20}$$

This equation related to the total electric value is the sampling value of this point, so we can obtain the MRTD equations based on Daubechies scaling function as following:

$$\begin{aligned} E^{\phi r,n+1}_{i+1/2,j,k} = & \frac{2\varepsilon-\sigma\Delta t}{2\varepsilon+\sigma\Delta t}E^{\phi r,n}_{i+1/2,j,k} + \frac{2\Delta t}{2\varepsilon+\sigma\Delta t}\frac{1}{(i+1/2)\,\Delta r\sin\left(j\Delta\theta\right)} \\ & \times\left\{\frac{1}{\Delta\theta}\sum_l a\left(l\right)\sin\left[\left(j+l+1/2\right)\Delta\theta\right]H^{\phi\varphi,\,n+1/2}_{i+1/2,j+l+1/2,k}\right. \\ & \left.-\frac{1}{\Delta\varphi}\sum_l a\left(l\right)H^{\phi\theta,\,n+1/2}_{i+1/2,j,k+l+1/2}\right\} \end{aligned} \tag{21}$$

$$\begin{aligned} E^{\phi\theta,n+1}_{i,j+1/2,k} = & \frac{2\varepsilon-\sigma\Delta t}{2\varepsilon+\sigma\Delta t}E^{\phi\theta,n}_{i,j+1/2,k} + \frac{2\Delta t}{2\varepsilon+\sigma\Delta t}\frac{1}{i\Delta r} \\ & \times\left\{\frac{1}{\sin\left[\left(j+1/2\right)\Delta\theta\right]\Delta\varphi}\sum_l a\left(l\right)H^{\phi r,\,n+1/2}_{i,j+1/2,k+l+1/2}\right. \\ & \left.-\sum_l a\left(l\right)\left(i+l+1/2\right)H^{\phi\varphi,\,n+1/2}_{i+l+1/2,j+1/2,k}\right\} \end{aligned} \tag{22}$$

$$E_{i,j,k+1/2}^{\phi\varphi,n+1} = \frac{2\varepsilon - \sigma\Delta t}{2\varepsilon + \sigma\Delta t} E_{i,j,k+1/2}^{\phi\varphi,n} + \frac{2\Delta t}{2\varepsilon + \sigma\Delta t} \frac{1}{i\Delta r} \left[\sum_l a(l)\,(i + l + 1/2)\, H_{i+l+1/2,j,k+1/2}^{\phi\theta,\, n+1/2} - \frac{1}{\Delta\theta} \sum_l a(l) H_{i,j+l+1/2,k+1/2}^{\phi r,\, n+1/2} \right] \tag{23}$$

$$H_{i,j+1/2,k+1/2}^{\phi r,n+1/2} = \frac{2\mu - \sigma_m\Delta t}{2\mu + \sigma_m\Delta t} H_{i,j+1/2,k+1/2}^{\phi r,n-1/2} - \frac{2\Delta t}{2\mu + \sigma_m\Delta t} \frac{1}{i\Delta r \sin\left[(j + 1/2)\,\Delta\theta\right]} \times \left\{ \frac{1}{\Delta\theta} \sum_l a(l) \sin\left[(j + l + 1)\,\Delta\theta\right] E_{i,j+l+1,k+1/2}^{\phi\varphi,\, n} - \frac{1}{\Delta\varphi} \sum_l a(l) E_{i,j+1/2,k+l+1}^{\phi\theta,\, n} \right\} \tag{24}$$

$$H_{i+1/2,j,k+1/2}^{\phi\theta,n+1/2} = \frac{2\mu - \sigma_m\Delta t}{2\mu + \sigma_m\Delta t} H_{i+1/2,j,k+1/2}^{\phi\theta,n-1/2} - \frac{2\Delta t}{2\mu + \sigma_m\Delta t} \frac{1}{(i+1/2)\,\Delta r} \left[\frac{1}{\sin(j\Delta\theta)\,\Delta\varphi} \sum_l a(l) E_{i+1/2,j,k+l+1}^{\phi r,\, n} - \sum_l a(l)\,(i + l + 1)\, E_{i+l+1,j,k+1/2}^{\phi\varphi,\, n} \right] \tag{25}$$

$$H_{i+1/2,j+1/2,k}^{\phi\varphi,n+1/2} = \frac{2\mu - \sigma_m\Delta t}{2\mu + \sigma_m\Delta t} H_{i+1/2,j+1/2,k}^{\phi\varphi,n-1/2} - \frac{2\Delta t}{2\mu + \sigma_m\Delta t} \frac{1}{(i+1/2)\,\Delta r} \left[\sum_l a(l)\,(i + l + 1)\, E_{i+l+1,j+1/2,k}^{\phi\theta,\, n} - \frac{1}{\Delta\theta} \sum_l a(l) E_{i+1/2,j+l+1,k}^{\phi r,\, n} \right] \tag{26}$$

As shown in Fig. 3, assuming that the total meshes are $N_r \times (N_\theta + 1) \times (N_\varphi + 1)$, due to the characteristic of the components in the MRTD equations, when $i = 0,\ 1,\ 2$ or $j = 0,\ 1,\ 2,\ N_\theta - 2,\ N_\theta - 1,\ N_\theta$ or $k = 0,\ 1,\ 2,\ N_\varphi - 2,\ N_\varphi - 1,\ N_\varphi$, some of the $\mathbf{E}$ and $\mathbf{H}$ fields need to be disposed particularly.

Firstly, observing Eq. (21), it is noted that when $j = 0$ or N_θ, the value of E_r is singular. And this problem can be solved via Ampere's

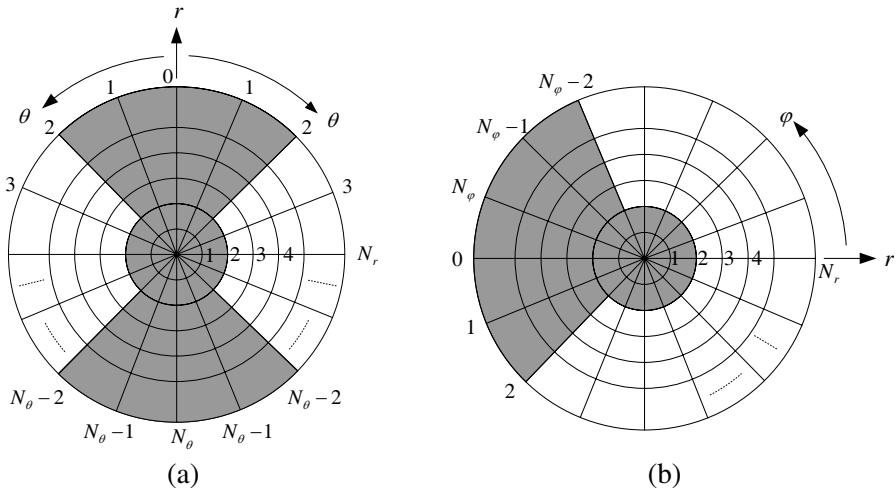

Figure 3. Area needs to be particularly treated (dark parts). (a) The r-θ-plane. (b) The r-φ-plane.

law [23]:

$$\oint_L \mathbf{H} \cdot dl = \iint_s \left(\varepsilon \frac{\partial}{\partial t} \mathbf{E} + \sigma \mathbf{E} \right) \cdot d\mathbf{s} \tag{27}$$

where the contour L is the circle defined by $j = 1/2$ or $N_\theta - 1/2$. Taking the integral of (27), we can get the formula for updating E_r at $j = 0$

$$E^{\phi r,\, n+1}_{i+1/2,0,k} = \frac{2\varepsilon - \sigma\Delta t}{2\varepsilon + \sigma\Delta t} E^{\phi r,\, n}_{i+1/2,0,k} + \frac{\sin(\Delta\theta/2)\,\Delta\varphi\Delta t}{(2\varepsilon + \sigma\Delta t)\,(i+1/2)\,\Delta r\,[1-\cos(\Delta\theta/2)]\,\pi} \sum_j H^{\phi\varphi,n+1/2}_{i+1/2,1/2,k} \tag{28}$$

At $j = N_\theta$, the formula is

$$E^{\phi r,\, n+1}_{i+1/2,N_\theta,k} = \frac{2\varepsilon - \sigma\Delta t}{2\varepsilon + \sigma\Delta t} E^{\phi r,\, n}_{i+1/2,N_\theta,k} - \frac{\sin(\Delta\theta/2)\,\Delta\varphi\Delta t}{(2\varepsilon + \sigma\Delta t)\,(i+1/2)\,\Delta r\,[1-\cos(\Delta\theta/2)]\,\pi} \sum_j H^{\phi\varphi,n+1/2}_{i+1/2,N_\theta-1/2,k} \tag{29}$$

Moreover, when $j = 1,\ 2,\ N_\theta - 2,\ N_\theta - 1,\ N_\theta$ or $k = 0,\ 1,\ 2,\ N_\varphi - 2,\ N_\varphi - 1,\ N_\varphi$, E_r should be treated particularly. Taking the spatial point

$((i+1/2)\,\Delta r, \Delta\theta, 0)$ as example, the updating equation of E_r is

$$E_{i+1/2,1,0}^{\phi r,n+1} = \frac{2\varepsilon-\sigma\Delta t}{2\varepsilon+\sigma\Delta t}E_{i+1/2,1,0}^{\phi r,n} + \frac{2\Delta t}{2\varepsilon+\sigma\Delta t}\frac{1}{(i+1/2)\,\Delta r\sin(\Delta\theta)} \times\left\{\frac{1}{\Delta\theta}\begin{bmatrix} a(0)\left(\sin((1+0{+}1/2)\,\Delta\theta)\,H_{i+1/2,1+0+1/2,0}^{\phi\varphi,\,n+1/2}\right. \\ \left.-\sin((1-1{+}1/2)\,\Delta\theta)\,H_{i+1/2,1-1+1/2,0}^{\phi\varphi,\,n+1/2}\right) \\ +a(1)\left(\sin((1+1{+}1/2)\,\Delta\theta)\,H_{i+1/2,1+1+1/2,0}^{\phi\varphi,\,n+1/2}\right. \\ \left.+\sin((1-2{+}1/2)\,\Delta\theta)\,H_{i+1/2,-(1-2+1/2),N_\varphi/2}^{\phi\varphi,\,n+1/2}\right) \\ +a(2)\left(\sin((1+2{+}1/2)\,\Delta\theta)\,H_{i+1/2,1+2,0}^{\phi\varphi,\,n+1/2}\right. \\ \left.+\sin((1-3{+}1/2)\,\Delta\theta)\,H_{i+1/2,-(1-3+1/2),N_\varphi/2}^{\phi\varphi,\,n+1/2}\right)\end{bmatrix} -\frac{1}{\Delta\varphi}\begin{bmatrix} a(0)\left(H_{i+1/2,1,0+1/2}^{\phi\theta,\,n+1/2}-H_{i+1/2,1,N_\varphi+1/2}^{\phi\theta,\,n+1/2}\right) \\ +a(1)\left(H_{i+1/2,1,1+1/2}^{\phi\theta,\,n+1/2}-H_{i+1/2,1,N_\varphi-1/2}^{\phi\theta,\,n+1/2}\right) \\ +a(2)\left(H_{i+1/2,1,2+1/2}^{\phi\theta,\,n+1/2}-H_{i+1/2,1,N_\varphi-3/2}^{\phi\theta,\,n+1/2}\right)\end{bmatrix}\right\} \quad (30)$$

that is

$$E_{i+1/2,1,0}^{\phi r,n+1} = \frac{2\varepsilon-\sigma\Delta t}{2\varepsilon+\sigma\Delta t}E_{i+1/2,1,0}^{\phi r,n} + \frac{2\Delta t}{2\varepsilon+\sigma\Delta t}\frac{1}{(i+1/2)\,\Delta r\sin(\Delta\theta)} \times\left\{\frac{1}{\Delta\theta}\begin{bmatrix} a(0)\left(\sin\left(\frac{3}{2}\Delta\theta\right)H_{i+1/2,3/2,0}^{\phi\varphi,\,n+1/2}-\sin\left(\frac{1}{2}\Delta\theta\right)H_{i+1/2,1/2,0}^{\phi\varphi,\,n+1/2}\right) \\ +a(1)\left(\sin\left(\frac{5}{2}\Delta\theta\right)H_{i+1/2,5/2,0}^{\phi\varphi,\,n+1/2}-\sin\left(\frac{1}{2}\Delta\theta\right)H_{i+1/2,1/2,N_\varphi/2}^{\phi\varphi,\,n+1/2}\right) \\ +a(2)\left(\sin\left(\frac{7}{2}\Delta\theta\right)H_{i+1/2,7/2,0}^{\phi\varphi,\,n+1/2}-\sin\left(\frac{3}{2}\Delta\theta\right)H_{i+1/2,3/2,N_\varphi/2}^{\phi\varphi,\,n+1/2}\right)\end{bmatrix} -\frac{1}{\Delta\varphi}\begin{bmatrix} a(0)\left(H_{i+1/2,1,1/2}^{\phi\theta,\,n+1/2}-H_{i+1/2,1,N_\varphi+1/2}^{\phi\theta,\,n+1/2}\right) \\ +a(1)\left(H_{i+1/2,1,3/2}^{\phi\theta,\,n+1/2}-H_{i+1/2,1,N_\varphi-1/2}^{\phi\theta,\,n+1/2}\right) \\ +a(2)\left(H_{i+1/2,1,5/2}^{\phi\theta,\,n+1/2}-H_{i+1/2,1,N_\varphi-3/2}^{\phi\theta,\,n+1/2}\right)\end{bmatrix}\right\} \quad (31)$$

Next, observing Eq. (22), it is obvious that when $i=0$, the value of E_θ is also singular. A simple method to treat this problem is let $E_\theta = 0$, which is feasible if the origin of the coordinate system is occupied by a perfect conductor. Another possible way is transform the E_θ fields at $i=0$ to Cartesian coordinates, and then transform back to spherical coordinates.

Furthermore, when $i = 1,\ 2$ or $k = 0,\ 1,\ 2,\ N_\varphi - 2,\ N_\varphi - 1,\ N_\varphi$, E_θ should be treated particularly. Taking the spatial point $(\Delta r, (j + 1/2)\,\Delta\theta, 0)$ as example, the updating equation of E_θ is

$$E^{\phi\theta,n+1}_{1,j+1/2,0} = \frac{2\varepsilon - \sigma\Delta t}{2\varepsilon + \sigma\Delta t} E^{\phi\theta,n}_{1,j+1/2,0} + \frac{2\Delta t}{2\varepsilon + \sigma\Delta t}\frac{1}{\Delta r}$$
$$\times \left\{ \frac{1}{\sin\left[(j + 1/2)\,\Delta\theta\right]\Delta\varphi} \begin{bmatrix} a\,(0)\left(H^{\phi r,\ n+1/2}_{1,j+1/2,1/2} - H^{\phi r,\ n+1/2}_{1,j+1/2,N_\varphi+1/2}\right) \\ +a\,(1)\left(H^{\phi r,\ n+1/2}_{1,j+1/2,3/2} - H^{\phi r,\ n+1/2}_{1,j+1/2,N_\varphi-1/2}\right) \\ +a\,(2)\left(H^{\phi r,\ n+1/2}_{1,j+1/2,5/2} - H^{\phi r,\ n+1/2}_{1,j+1/2,N_\varphi-3/2}\right) \end{bmatrix} \right.$$
$$\left. - \begin{bmatrix} a\,(0)\left(\frac{3}{2}H^{\phi\varphi,\ n+1/2}_{3/2,j+1/2,0} - \frac{1}{2}H^{\phi\varphi,\ n+1/2}_{1/2,j+1/2,0}\right) \\ +a\,(1)\left(\frac{5}{2}H^{\phi\varphi,\ n+1/2}_{5/2,j+1/2,0} - \frac{3}{2}H^{\phi\varphi,\ n+1/2}_{1/2,j+1/2,N_\varphi}\right) \\ +a\,(2)\left(\frac{7}{2}H^{\phi\varphi,\ n+1/2}_{7/2,j+1/2,0} - \frac{5}{2}H^{\phi\varphi,\ n+1/2}_{5/2,j+1/2,N_\varphi}\right) \end{bmatrix} \right\} \tag{32}$$

Referring to Eq. (23), the treatment of E_φ at $i = 0$ or $j = 0,\ N_\theta$ is the same with E_θ. And when $i = 1,\ 2$ or $j = 1,\ 2,\ N_\theta - 2,\ N_\theta - 1,\ E_\theta$ also should be treated particularly. Taking the spatial point $(\Delta r,\ \Delta\theta, (k + 1/2)\,\Delta\varphi)$ as example, the updating equation of E_φ is

$$E^{\phi\varphi,n+1}_{1,1,k+1/2} = \frac{2\varepsilon - \sigma\Delta t}{2\varepsilon + \sigma\Delta t} E^{\phi\varphi,n}_{1,1,k+1/2} + \frac{2\Delta t}{2\varepsilon + \sigma\Delta t}\frac{1}{\Delta r}$$
$$\times \left\{ \begin{bmatrix} a\,(0)\left(\frac{3}{2}H^{\phi\theta,\ n+1/2}_{3/2,1,k+1/2} - \frac{1}{2}H^{\phi\theta,\ n+1/2}_{1/2,1,k+1/2}\right) \\ +a\,(1)\left(\frac{5}{2}H^{\phi\theta,\ n+1/2}_{5/2,1,k+1/2} - \frac{1}{2}H^{\phi\theta,\ n+1/2}_{1/2,1,k+1/2-N_\varphi/2}\right) \\ +a\,(2)\left(\frac{7}{2}H^{\phi\theta,\ n+1/2}_{7/2,1,k+1/2} - \frac{3}{2}H^{\phi\theta,\ n+1/2}_{3/2,1,k+1/2-N_\varphi/2}\right) \end{bmatrix} \right.$$
$$\left. - \frac{1}{\Delta\theta} \begin{bmatrix} a\,(0)\left(H^{\phi r,\ n+1/2}_{1,3/2,k+1/2} - H^{\phi r,\ n+1/2}_{1,1/2,k+1/2}\right) \\ +a\,(1)\left(H^{\phi r,\ n+1/2}_{1,5/2,k+1/2} - H^{\phi r,\ n+1/2}_{1,1/2,k+1/2-N_\varphi/2}\right) \\ +a\,(2)\left(H^{\phi r,\ n+1/2}_{1,7/2,k+1/2} - H^{\phi r,\ n+1/2}_{1,3/2,k+1/2-N_\varphi/2}\right) \end{bmatrix} \right\} \tag{33}$$

The treatment of the **H** fields at the proposed special points is similar with the **E** fields, and can be obtained by duality.

3. STABILITY AND DISPERSION ANALYSIS

3.1. Stability Analysis

In this section, it is assumed throughout the stability and dispersion analysis that the **E** and **H** fields are expanded only in terms of scaling functions (S-MRTD) in space domain [24]. Following the procedure of [1], the MRTD equations for the 2-D TM mode can be written as

$$\frac{H_{r,i,j+1/2}^{n+1/2} - H_{r,i,j+1/2}^{n-1/2}}{\Delta t} = -\frac{\sum_l a(l) \sin[(j+l+1)\,\Delta\theta] E_{\varphi,i,j+l+1}^{n}}{\mu i \Delta r \sin[(j+1/2)\,\Delta\theta]} \tag{34}$$

$$\frac{H_{\theta,i+1/2,j}^{n+1/2} - H_{\theta,i+1/2,j}^{n-1/2}}{\Delta t} = \frac{\sum_l a(l)\,(i+l+1)\,E_{\varphi,i+l+1,j}^{n}}{\mu\,(i+1/2)\,\Delta r} \tag{35}$$

$$\frac{E_{\varphi,i,j}^{n+1} - E_{\varphi,i,j}^{n}}{\Delta t} = \frac{1}{i\Delta r}\left[\sum_l a(l)\,(i+l+1/2)\,H_{\theta,i+l+1/2,j}^{n+1/2} - \frac{1}{\Delta\theta}\sum_l a(l) H_{r,\,i,j+l+1/2}^{n+1/2}\right] \tag{36}$$

Following the stability analysis described in [25], the finite-difference approximations of the time derivatives on the left-hand side of the equations can be written as an eigenvalue problem

$$\frac{H_{r,i,j+1/2}^{n+1/2} - H_{r,i,j+1/2}^{n-1/2}}{\Delta t} = \lambda H_{r,i,j+1/2}^{n} \tag{37}$$

$$\frac{H_{\theta,i+1/2,j}^{n+1/2} - H_{\theta,i+1/2,j}^{n-1/2}}{\Delta t} = \lambda H_{\theta,i+1/2,j}^{n} \tag{38}$$

$$\frac{E_{\varphi,i,j}^{n+1} - E_{\varphi,i,j}^{n}}{\Delta t} = \lambda E_{\varphi,i,j}^{n+1/2} \tag{39}$$

In order to avoid instability during normal time stepping, the imaginary part of λ, $\mathrm{Im}(\lambda)$, must satisfy

$$-\frac{2}{\Delta t} \le \mathrm{Im}(\lambda) \le \frac{2}{\Delta t} \tag{40}$$

Assuming that the medium of the calculating space is homogeneous, lossless and non-magnetic, so any monochromatic plane wave can be indicated by the referred form [26]

$$H_{r,I,J} = H_{r_0} \exp[-j(k_r I\Delta r + k_\theta J\Delta r\Delta\theta)]$$
$$H_{\theta,I,J} = H_{\theta_0} \exp[-j(k_r I\Delta r + k_\theta J\Delta r\Delta\theta)]$$
$$E_{\varphi,I,J} = E_{\varphi_0} \exp[-j(k_r I\Delta r + k_\theta J\Delta r\Delta\theta)]$$

Substituting these expressions to (37)–(39) and applying Euler's identity, we get

$$\lambda^2 = \left\{ \frac{1}{\Delta r} \left[\sum_{i'=0}^{2} a\left(i'\right) \sin\left(k_r \Delta r \left(i' + \frac{1}{2} \right) \right) \right] \right\}^2 + \left\{ \frac{2}{\Delta r \Delta \theta} \left[\sum_{j'=0}^{2} a\left(j'\right) \sin\left(k_\theta \frac{\Delta r \Delta \theta}{2} \left(j' + \frac{1}{2} \right) \right) \right] \right\}^2 \quad (41)$$

In (41), λ is a pure imaginary, which is bounded for any wave vector $k = (k_r, k_\theta)$

$$-2c \left(\sum_{i'=0}^{2} a\left(i'\right) \right) \left(\frac{1}{(\Delta r)^2} + \frac{4}{(\Delta r \Delta \theta)^2} \right)^{\frac{1}{2}} \leq \mathrm{Im}(\lambda) \leq 2c \left(\sum_{i'=0}^{2} a\left(i'\right) \right) \left(\frac{1}{(\Delta r)^2} + \frac{4}{(\Delta r \Delta \theta)^2} \right)^{\frac{1}{2}} \quad (42)$$

where $c = 1/\sqrt{\mu\varepsilon}$ is the speed of the light.

Numerical stability is maintained for every spatial mode only when the range of eigenvalues given by (42) is contained entirely within the stable range of time-differentiation eigenvalues given by (40). Since both ranges are symmetrical around zero, it is adequate to set the upper bound of (42) to be smaller or equal to (40), giving

$$\Delta t \leq \frac{S}{c\sqrt{\frac{1}{(\Delta r)^2} + \frac{4}{(\Delta r \Delta \theta)^2}}} \quad (43)$$

where

$$S = \frac{1}{\left[\sum_{i'=0}^{2} a\left(i'\right) \right]} \approx 0.8727 \quad (44)$$

It is known that

$$\Delta t_{\mathrm{FDTD}} \leq \frac{1}{c\sqrt{\frac{1}{(\Delta r)^2} + \frac{4}{(\Delta r \Delta \theta)^2}}} \quad (45)$$

Equations (43)–(45) show that for the same discretization size it is not advantageous to choose time step at the stability limit for MRTD scheme compared with that for the FDTD scheme. However, as introduced in the next section, this can be largely compensated by

the better dispersion performance given by MRTD (for large cells). The stability analysis can be generalized easily to three dimensions

$$\Delta t \leq \frac{S}{c\sqrt{\frac{1}{\Delta r^2}+\frac{4}{(\Delta r\Delta\theta)^2}+\frac{4}{(\Delta r\Delta\varphi\sin\Delta\theta)^2}}} \tag{46}$$

3.2. Dispersion Analysis

In this section, the numerical dispersion of the MRTD scheme is investigated and compared to that of the standard FDTD. The dispersion relation was obtained by substituting a time-harmonic trial solution into the update equations and numerically solving the resulting nonlinear equation

$$\begin{aligned}\left[\frac{1}{c\Delta t}\sin\left(\frac{\omega\Delta t}{2}\right)\right]^2 &= \left\{\frac{1}{\Delta r}\left[\sum_{i'=0}^{2} a\left(i'\right)\sin\left(k_r\left(i'+\frac{1}{2}\right)\Delta r\right)\right]\right\}^2 \\ &+ \left\{\frac{1}{r'\Delta\theta}\left[\sum_{j'=0}^{2} a\left(j'\right)\sin\left(k_\theta r'\left(j'+\frac{1}{2}\right)\Delta\theta\right)\right]\right\}^2 \\ &+ \left\{\frac{1}{r'\Delta\varphi\sin\Delta\theta}\left[\sum_{k'=0}^{2} a\left(k'\right)\sin\left(k_\varphi r'\Delta\varphi\left(k'+\frac{1}{2}\right)\sin\Delta\theta\right)\right]\right\}^2 \end{aligned} \tag{47}$$

where ω corresponds to the wave angular frequency, r' to the radial location and $k_{r,\theta,\varphi}$ to the r, θ, φ-components of the numerical wave vector respectively. Apparently, the equation above shows that the numerical dispersion of MRTD has the relationships with the time-step, cell size, wave frequency, radial location and propagation direction. Since it is difficult to treat the 3-D dispersion case, for the sake of easily illustrating, a 2-D case in the θ-φ-plane is discussed. Assuming that the Courant-Friedrichs-Lewy number (CFLN) $c\Delta t/\delta = p$, $\omega\Delta t = \Omega$ and $r'\Delta\theta = r'\Delta\varphi\sin\Delta\theta = \delta$, then Eq. (47) can be rewritten as

$$\Omega = 2\arcsin\left\{p\sqrt{\begin{aligned}&\left[\sum_{j'=0}^{2} a\left(j'\right)\sin\left(k_\theta\delta\left(j'+\tfrac{1}{2}\right)\right)\right]^2 \\ &+\left[\sum_{k'=0}^{2} a\left(k'\right)\sin\left(k_\varphi\delta\left(k'+\tfrac{1}{2}\right)\right)\right]^2\end{aligned}}\right\} \tag{48}$$

To satisfy the stability requirements, p has to be smaller than $0.6171\ (= 0.8727/\sqrt{2})$ for the 2-D simulations.

In Fig. 4, the normalized frequency Ω is plotted with respect to the normalized wavenumber $X = |\mathbf{k}|\delta$ for a value of $p = 0.1$, where $\mathbf{k}$ is

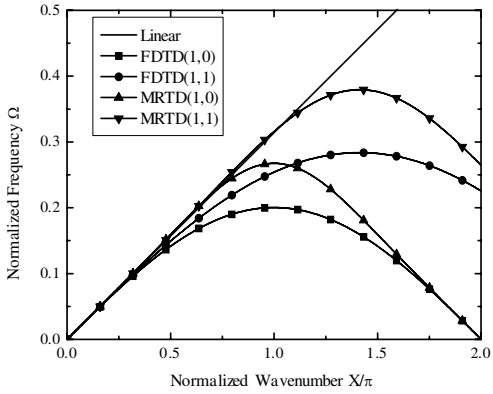

Figure 4. Dispersion diagram.

the wave vector (k_θ, k_φ). For wave propagation in (1, 0) direction, we have used $k_\varphi = 1$ and $k_z = 0$. Similarly, for wave propagation in (1, 1) direction, we have used $k_\varphi = k_z = 1$. This figure illustrates the highly linear dispersion characteristic of the MRTD based on Daubechies wavelet in comparison with the dispersion characteristics of FDTD schemes, which implies that the MRTD scheme can keep a better accuracy when there are less grid points.

In order to permit determination of **k** for any wave-propagation direction, here we define

$$\mathbf{k} = (k_r, k_\theta, k_\varphi) = k_0 \left(\cos\alpha, \sin\alpha\cos\beta, \sin\alpha\sin\beta\right)$$

where (α, β) is the azimuth angle in spherical coordinates. Following the procedure of [25], the Eq. (47) can be written as

$$\frac{\omega^2}{c^2} = (k_0\cos\alpha)^2 \frac{\left[\sum\limits_{i'=0}^{2} a\left(i'\right)\sin\left(k_0\left(i'+\frac{1}{2}\right)\Delta r\cos\alpha\right)\right]^2}{\left(\frac{k_0\Delta r\cos\alpha}{2}\right)^2}$$

$$+ (k_0\sin\alpha\cos\beta)^2 \frac{\left[\sum\limits_{j'=0}^{2} a\left(j'\right)\sin\left(k_0\rho'\left(j'+\frac{1}{2}\right)\Delta\theta\sin\alpha\cos\beta\right)\right]^2}{\left(\frac{k_0\rho'\Delta\theta\sin\alpha\cos\beta}{2}\right)^2}$$

$$+ (k_0\sin\alpha\sin\beta)^2 \frac{\left[\sum\limits_{j'=0}^{2} a(k')\sin\left(k_0\rho'\left(k'+\frac{1}{2}\right)\Delta\varphi\sin\Delta\theta\sin\alpha\sin\beta\right)\right]^2}{\left(\frac{k_0\rho'\Delta\varphi\sin\Delta\theta\sin\alpha\sin\beta}{2}\right)^2} \quad (49)$$

since $k = \omega/v_p = 2\pi/\lambda_0$, where v_p is numerical phase velocity and λ_0 is the free-space wavelength, the Eq. (49) can be rewritten as

$$\left(\frac{v_p}{c}\right)^2 = \frac{\left[\sum_{i'=0}^{2} a\left(i'\right) \sin\left(\frac{2\pi\left(i'+\frac{1}{2}\right)\Delta r\cos\alpha}{\lambda_0}\right)\right]^2}{\left(\frac{\pi\Delta r\cos\alpha}{\lambda_0}\right)^2}\cos^2\alpha + \frac{\left[\sum_{j'=0}^{2} a\left(j'\right) \sin\left(\frac{2\pi\rho'\left(j'+\frac{1}{2}\right)\Delta\theta\sin\alpha\cos\beta}{\lambda_0}\right)\right]^2}{\left(\frac{\pi\rho'\Delta\theta\sin\alpha\cos\beta}{\lambda_0}\right)^2}\sin^2\alpha\cos^2\beta + \frac{\left[\sum_{j'=0}^{2} a(k') \sin\left(\frac{2\pi\rho'\sin\Delta\theta\sin\alpha\sin\beta\left(k'+\frac{1}{2}\right)\Delta\varphi}{\lambda_0}\right)\right]^2}{\left(\frac{\pi\rho'\sin\Delta\theta\sin\alpha\sin\beta}{\lambda_0}\right)^2}\sin^2\alpha\sin^2\beta \quad (50)$$

Also for the sake of easily illustrating, here we also discuss the 2-D case mentioned above, then the Eq. (50) can be written as

$$\left(\frac{v_p}{c}\right)^2 = \frac{\left[\sum_{i'=0}^{2} a\left(i'\right) \sin\left(\frac{2\pi\delta}{\lambda_0}\cos\beta\left(i'+\frac{1}{2}\right)\right)\right]^2}{\left(\frac{\pi\delta}{\lambda_0}\right)^2}\cos^2\beta + \frac{\left[\sum_{j'=0}^{2} a\left(j'\right) \sin\left(\frac{2\pi\delta}{\lambda_0}\sin\beta\left(j'+\frac{1}{2}\right)\right)\right]^2}{\left(\frac{\pi\delta}{\lambda_0}\right)^2}\sin^2\beta \quad (51)$$

Figure 5 illustrates the variation of v_p in MRTD and FDTD methods with propagation direction α. Here, two different grid-sampling densities λ_0/δ are examined for MRTD: $\lambda_0/\delta = 2$ points per λ_0 and $\lambda_0/\delta = 3$, two λ_0/δ for FDTD: $\lambda_0/\delta = 3$ and$\lambda_0/\delta = 15$. From this figure, it is can be easily seen that the MRTD can keep a higher accuracy with the same grid-sampling density than that of the FDTD, which also validates the conclusion above.

4. NUMERICAL RESULTS

To validate the benefits of the high linear dispersion characteristics of the proposed scheme, as Table 2 shows, the simulations results of

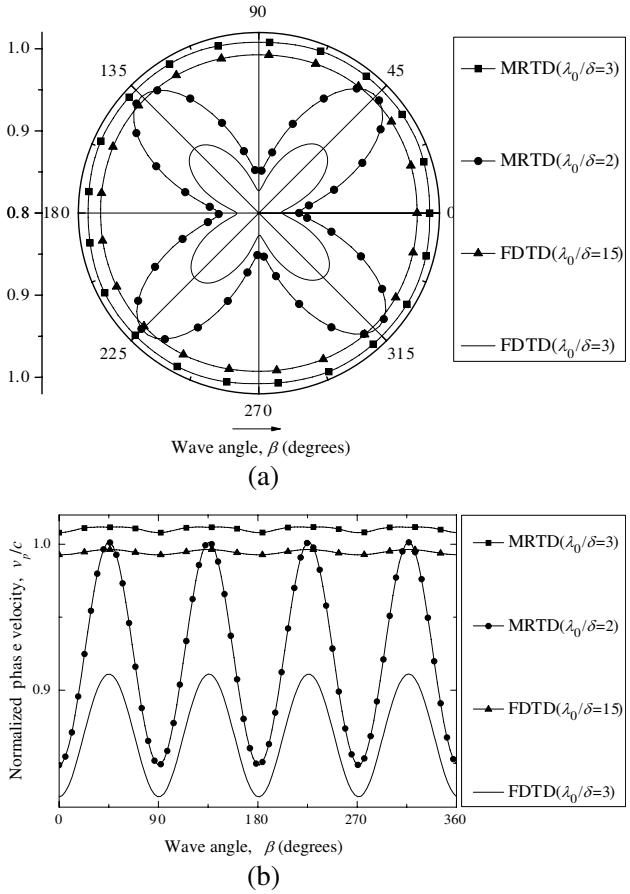

Figure 5. Variation of the numerical phase velocity with wave-propagation angle for 2-D MRTD and FDTD grids. (a) Illustrated by polar coordinates. (b) Illustrated by cartesian coordinates.

the resonant frequencies for an air-filled spherical resonator are given here. The radius of the cavity resonator is $r = 1\,\mathrm{m}$. Its theoretical resonant frequencies are readily available [27]. In the simulation using Yee's FDTD scheme, the computational domain was discretized using the grid with $\Delta\rho = 3.125\,\mathrm{cm}$, $\Delta\theta = \pi/48$ and $\Delta\varphi = \pi/24$, leading to a mesh of $32 \times 96 \times 48$ gird points. For the MRTD scheme, a grid with $\Delta\rho = 12.5\,\mathrm{cm}$, $\Delta\theta = \pi/12$, $\Delta\varphi = \pi/6$ and with a mesh of $8 \times 24 \times 12$ gird points, was chosen. Note that the time discretization interval $\Delta t = 4.421 \times 10^{-13}\,\mathrm{s}$ was chosen to be identical for both schemes in order to exploit the linearity of the dispersion characteristics for

Table 2. Simulation results.

Analytic values	MRTD		FDTD	
	Computed values	Relative errors	Computed values	Relative errors
131.01 MHz	131.01 MHz	0	130.76 MHz	−0.191%
292.06 MHz	292.43 MHz	0.127%	292.01 MHz	−0.017%
444.85 MHz	444.95 MHz	0.023%	444.33 MHz	−0.117%
596.16 MHz	597.39 MHz	0.206%	595.87 MHz	−0.049%
No. of iterations	65536		65536	
CPU time/s	33.23		1129.84	

MRTD. The excitation pulse is a Gaussian pulse which is defined as

$$E_i(t) = \exp\left[-4\pi(t - t_0)/\tau\right]^2 \tag{52}$$

where $t_0 = \tau = 2.0\,\text{ns}$. Compared with the FDTD method, the total number of grid points is reduced by a factor of 64, and the execution time for the analysis was reduced by a factor of 34 for MRTD method. In addition, note that for the MRTD scheme, the relative error of the resonant frequencies is positive which corresponds to an overestimation of the resonant frequencies. For FDTD scheme, the relative error of the resonant frequencies is negative corresponding to an underestimation of the resonant frequencies. This is exactly what has to be expected from the dispersion diagrams (see Figs. 4–5).

Since the use of Daubechies basis functions does not allow localized boundary conditions, as Fig. 6 shows, here we apply the image technique to the perfect electric conductor (PEC) boundary [1].

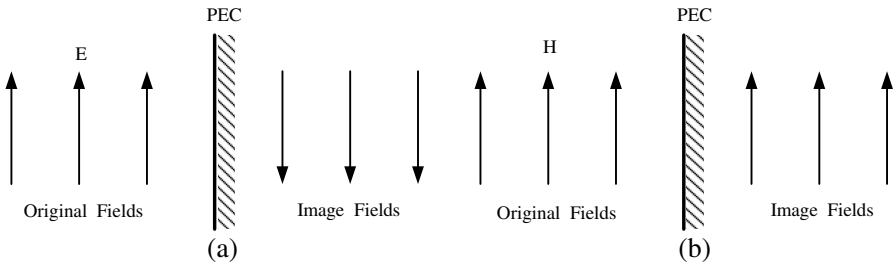

Figure 6. Original and image fields of the MRTD lattice with respect to PEC boundary.

Next, a 3-D spherical case in free space about the field radiated from a electric dipole source is simulated with FDTD and MRTD schemes. Following the procedure of [28], the perfectly matched layer (PML) can be easily derived for the proposed spherical MRTD grids (not shown for saving space). The computational domain for both FDTD and MRTD approaches is discretized using a $(N_r, N_\theta, N_\varphi) = (28, 10, 20)$ cell lattice with eight-cell-thick PML terminate the grid in r direction, and the PML region is terminated with a PEC wall. The source is a radiating electric dipole located at the grid point (3, 5, 0), and is characterized by

$$p(t) = 10^{-10} \exp\left[-(t - 3T)/T\right]^2 \tag{53}$$

where $T = 2.0\,\text{ns}$. It is easily demonstrated that such a dipole produces an electric field in time domain

$$E(\mathbf{r}, t) = \frac{\mu_0}{4\pi r}\left\{\mathbf{e}_r\left[\frac{c}{r}\frac{\partial}{\partial t} + \frac{c^2}{r^2}\right]2\cos\theta + \mathbf{e}_\theta\left[\frac{\partial^2}{\partial t^2} + \frac{c}{r}\frac{\partial}{\partial t} + \frac{c^2}{r^2}\right]\sin\theta\right\} p\left(t - \frac{c}{r}\right) \tag{54}$$

and the electric dipole source can be employed in the MRTD as following

$$E^{\phi\theta,n+1}_{3,5+1/2,0} = E^{\phi\theta,n}_{3,5+1/2,0} - \frac{\Delta t}{9\varepsilon_0 \Delta r^3 \Delta\theta\Delta\varphi \sin(5.5\Delta\theta)}\left(\frac{dp}{dt}\right)^{n+1/2} \tag{55}$$

First, we use an uniform cell discretization size in the r direction $\Delta r = 6\,\text{cm}$, a time discretization interval $\Delta t = 6.949 \times 10^{-12}\,\text{s}$ for both MRTD and FDTD schemes, and a receiver located at the grid point (13, 5, 0). As shown in Fig. 7, the curves for MRTD and FDTD methods are both in excellent agreement with the analytical curve. Then we use another uniform cell discretization size in the r direction $\Delta r = 30\,\text{cm}$, and a time discretization interval $\Delta t = 3.476 \times 10^{-11}\,\text{s}$ for both MRTD and FDTD schemes. For simplicity, the receiver is also located at (13, 5, 0). As Fig. 8(a) shows, we can see that the curve for FDTD method is absolutely distortional, which implies that the grid-sampling density is too low for the FDTD technique. However, as illustrated in Fig. 8(b), unlike the FDTD scheme, the curve for MRTD scheme can be still in good agreement with the analytical curve. The results visibly validate the conclusion in Section 3. Moreover, it is noticed that in Fig. 8(b) there is little oscillation for the E_θ field in the MRTD simulation, the residual field can be attributed to three major sources: discretization error of the sphere model, numerical dispersion effect due to the high grid curvature in the simulation region, and the PML reflection.

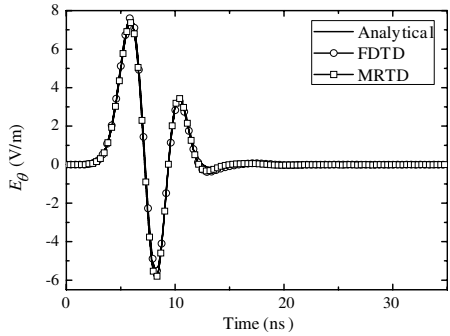

Figure 7. Analytical solution for the electric dipole versus 3-D spherical-grid FDTD and MRTD solutions.

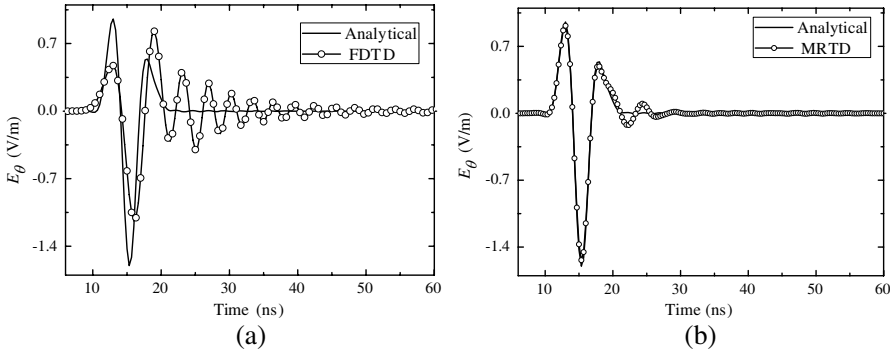

Figure 8. Analytical solution versus FDTD and MRTD solutions. (a) Analytical solution for the electric dipole versus 3-D spherical-grid FDTD solutions. (b) Analytical solution for the electric dipole versus 3-D spherical-grid MRTD solutions.

5. CONCLUSION

This paper has developed an MRTD algorithm based on Daubechies' scaling functions with a spherical grid. The stability and dispersion property of the scheme is also investigated. It is shown that the larger cells can decrease the numerical phase error with the scheme, which makes it significantly lower than FDTD for low and medium discretizations. Furthermore, numerical verifications are presented to demonstrate the validity of the proposed method, and it is indicated that at the acceptable accuracy level, the proposed method can greatly save the CPU memory and computational time compared with the

conventional FDTD method. MRTD codes are then developed based on the time-domain versions of the equations.

ACKNOWLEDGMENT

The authors would like to thank the reviewers for helpful remarks.

REFERENCES

1. Krumpholz, M. and L. P. B. Katehi, "MRTD: New time-domain schemes based on multiresolution analysis," *IEEE Trans. Microwave Theory Tech.*, Vol. 44, No. 4, 555–561, Apr. 1996.
2. Sirenko, K., V. Pazynin, Y. K. Sirenko, and H. Bağci, "An FFT-accelerated FDTD scheme with exact absorbing conditions for characterizing axially symmetric resonant structures," *Progress In Electromagnetics Research*, Vol. 111, 331–364, 2011.
3. Lee, K. H., I. Ahmed, R. S. M. Goh, E. H. Khoo, E. P. Li, and T. G. G. Hung, "Implementation of the FDTD method based on Lorentz-Drude dispersive model on GPU for plasmonics applications," *Progress In Electromagnetics Research*, Vol. 116, 441–456, 2011.
4. Izadi, M., M. Z. A. Ab Kadir, and C. Gomes, "Evaluation of electromagnetic fields associated with inclined lightning channel using second order FDTD-hybrid methods," *Progress In Electromagnetics Research*, Vol. 117, 209–236, 2011.
5. Vaccari, A., A. Cala' Lesina, L. Cristoforetti, and R. Pontalti, "Parallel implementation of a 3D subgridding FDTD algorithm for large simulations," *Progress In Electromagnetics Research*, Vol. 120, 263–292, 2011.
6. Kong, Y.-D. and Q.-X. Chu, "Reduction of numerical dispersion of the six-stages split-step unconditionally-stable FDTD method with controlling parameters," *Progress In Electromagnetics Research*, Vol. 122, 175–196, 2012.
7. Kong, L.-Y., J. Wang, and W.-Y. Yin, "A novel dielectric conformal FDTD method for computing sar distribution of the human body in a metallic cabin illuminated by an intentional electromagnetic pulse (IEMP)," *Progress In Electromagnetics Research*, Vol. 126, 355–373, 2012.
8. Mao, Y., B. Chen, H.-Q. Liu, J.-L. Xia, and J.-Z. Tang, "A hybrid implicit-explicit spectral FDTD scheme for oblique incidence problems on periodic structures," *Progress In Electromagnetics Research*, Vol. 128, 153–170, 2012.

9. Wang, J.-B., B.-H. Zhou, L.-H. Shi, C. Gao, and B. Chen, "A novel 3-D weakly conditionally stable FDTD algorithm," *Progress In Electromagnetics Research*, Vol. 130, 525–540, 2012.
10. Xiong, R., B. Chen, Y. Mao, B. Li, and Q.-F. Jing, "A simple local approximation FDTD model of short apertures with a finite thickness," *Progress In Electromagnetics Research*, Vol. 131, 135–152, 2012.
11. Xiong, R., B. Chen, J.-J. Han, Y.-Y. Qiu, W. Yang, and Q. Ning, "Transient resistance analysis of large grounding systems using the FDTD method," *Progress In Electromagnetics Research*, Vol. 132, 159–175, 2012.
12. Gradoni, G., V. Mariani Primiani, and F. Moglie, "Reverberation chamber as a multivariate process: FDTD evaluation of correlation matrix and independent positions," *Progress In Electromagnetics Research*, Vol. 133, 217–234, 2013.
13. Kong, Y.-D., Q.-X. Chu, and R.-L. Li, "High-order unconditionally-stable four-step ADI-FDTD methods and numerical analysis," *Progress In Electromagnetics Research*, Vol. 135, 713–734, 2013.
14. Chun, K., H. Kim, H. Kim, and Y. Chung, "PLRC and ADE implementations of Drude-critical point dispersive model for the FDTD method," *Progress In Electromagnetics Research*, Vol. 135, 373–390, 2013.
15. Stefanski, T. P., "Implementation of FDTD-compatible Green's function on heterogeneous CPU-GPU parallel processing system," *Progress In Electromagnetics Research*, Vol. 135, 297–316, 2013.
16. Wang, W., P.-G. Liu, and Y.-J. Qin, "An unconditional stable 1D-FDTD method for modeling transmission lines based on precise split-step scheme," *Progress In Electromagnetics Research*, Vol. 135, 245–260, 2013.
17. Donelli, M., I. Craddock, D. Gibbins, and M. Sarafianou, "A three dimensional time domain microwave imaging method for breast cancer detection based on an evolutionary algorithm," *Progress In Electromagnetic Research M*, Vol. 18, 193–195, 2011.
18. Johnson, J., T. Takenaka, K. A. Hong Ping, S. Honda, and T. Tanaka, "Advances in the 3-D forward-backward time stepping (FBTS) inverse scattering technique for breast cancer detection," *IEEE Trans. Biomed. Eng.*, Vol. 56, No. 9, 2232–2243, 2009.
19. Moriyama, T., T. Takenaka, and Z. Meng, "Forward-backward time stepping method combined with genetic algorithm applied to breast cancer detection," *Microwave and Optical Technology Letters*, Vol. 53, No. 2, 438–442, 2009.

20. Cheong, Y. W., Y. M. Lee, K. H. Ra, J. G. Kang, and C. C. Shin, "Wavelet-Galerkin scheme of time-dependent inhomogeneous electromagnetic problems," *IEEE Microwave Guided Wave Lett.*, Vol. 9, No. 8, 297–299, Aug. 1999.
21. Fujii, M. and W. J. R. Hoefer, "Dispersion of time domain wavelet Galerkin method based on Daubechies' compactly supported scaling functions with three and four vanishing moments," *IEEE Microwave Guided Wave Lett.*, Vol. 10, No. 4, 125–127, Apr. 2000.
22. Sweldens, W. and R. Piessens, "Wavelet sampling techniques," *Proc. Statistical Computing Section*, 20–29, 1993.
23. Holland, R., "THREDS: A finite-difference time-domain EMP codein 3D spherical coordinates," *IEEE Trans. Nucl. Sci.*, Vol. 30, 4592–4595, 1983.
24. Tentzeris, E. M., R. L. Robertson, J. F. Harvey, and L. P. B. Katehi, "Stability and dispersion analysis of Battle-Lemarie-based MRTD schemes," *IEEE Trans. Microwave Theory Tech.*, Vol. 47, No. 7, 1004–1013, Jul. 1999.
25. Taflove, A., *Computational Electrodynamics: The Finite-difference Time-domain Method*, Artech House, Norwood, MA, 1995.
26. Shlager, K. L. and J. B. Schneider, "Comparison of the dispersion properties of higher order FDTD schemes and equivalent-sized MRTD schemes," *IEEE Trans. Antenna Propagat.*, Vol. 52, No. 4, 1095–1104, Apr. 2004.
27. Harrington, R. F., *Time-harmonic Electromagnetic Fields*, McGraw-Hill, New York, 1961.
28. Teixeira, F. L. and W. C. Chew, "PML-FDTD in cylindrical and spherical grids," *IEEE Microwave Guided Wave Lett.*, Vol. 7, No. 9, 285–287, Sep. 1997.